ENVELOPES OF PRE-MAIN SEQUENCE STARS

NASA Grant NAGW-2919

Annual Status Report No. 4

For the period 1 February 1995 through 31 January 1996

and

Final Report

For the period 1 February 1992 through 31 January 1996

Principal Investigator

Lee W. Hartmann

February 1996

Prepared for

National Aeronautics and Space Administration

Washington, D.C. 20546

Smithsonian Institution
Astrophysical Observatory
Cambridge, Massachusetts 02138

The Smithsonian Astrophysical Observatory
is a member of the
Harvard-Smithsonian Center for Astrophysics

The NASA Technical Officer for this Grant is Dr. Robert V. Stachnik, Code: SZ, **Headquarters, National Aerona**utics and Space Administration, Washington, D.C. 20546

Annual Report for NAGW-2919

SHEET MODELS OF PROTOSTELLAR COLLAPSE

Recognizing that protostellar clouds are unlikely to be completely spherical, we explore some effects of initial cloud geometry by considering collapse from a sheet initially in hydrostatic equilibrium. A qualitatively different feature of sheet collapse compared with spherical contraction is the development of relatively evacuated cavities in the infalling dusty cloud, which arise because material falls in first along the shortest dimension to the central gravitating mass. We introduce a flattening parameter η which joins our approach with that of Terebey *et al.* (1984); $\eta = 0$ corresponds exactly to that of Terebey *et al.* , while values of $\eta \sim 2 - 3$ are indicated for typical times during the collapse of the self-gravitating isothermal sheet. This analytic models reproduces the main features of our previous numerical time-dependent simulations (see Figure 1).

We performed detailed radiative transfer calculations which suggest that these collapse cavities can naturally explain the morphological appearance of many reflection nebulae around young stars on small distance scales without requiring initially diverging outflows (Figure 2). Sheet collapse models can simultaneously explain small-scale reflection nebula morphologies and dust envelope emission properties of many young stellar objects more easily than the standard spherical collapse models. The sheet collapse picture suggests that protostars, i.e. young stellar objects still accreting a large fraction of their mass from infalling envelopes, may be optically visible over a substantial range of system inclinations to the line of sight. These results may be especially relevant to cases where fragmentation and collapse has been triggered by an external impulse, such as a shock wave.

We showed how many properties of the flat-spectrum T Tauri star HL Tau can be intepreted in terms of flattened protostellar cloud collapse (Figure 3). Overall, our model explains the main features of the flattened infalling gas cloud found by Hayashi *et al.* (1993) from ^{13}CO interferometric mapping, the scattered light nebulae observed by Beckwith *et al.* (1989) and Beckwith & Birk (1995), the redshifted C_2 absorption found by Grasdalen *et al.* (1989), and the flat-spectral energy distribution (Calvet *et al.* 1994). The model cannot reproduce all of the fine detail seen in the Hubble Space Telescope image of HL Tau (Stapelfeldt et al. 1995), but these observations are more consistent with an infall model than with a disk.

References

Beckwith, S.V.W., & Birk, C.C. 1995, ApJ, 449, L59

Beckwith, S.V.W., Sargent, A.I., Koresko, C.D., & Weintraub, D.A. 1989, ApJ, 343, 393

Calvet, N., Hartmann, L., Kenyon, S., & Whitney, B. 1994, ApJ, 434, 330

Grasdalen, G.L., Sloan, G., Stout, M., Strom, S.E., & Welty, A.D. 1989, ApJL, 339, L37
Hayashi, M., Ohashi, N., & Miyama, S. 1993, ApJ, 418, L71
Stapelfeldt, K.R., Burrows, C.J., Krist, J.E., Trauger, J.T., Hester, J.J., Holtzman, J.A., Ballester, G.E., Casertano, S., Clarke, J.T., Cristp, D., Evans, R.W., Gallagher, J.S. III, Griffiths, R.E., Hoessel, J.G., Mould, J.R., Scowen, P.A., Watson, A.M., & Westphal, J.A. 1995, ApJ, L Aug 20.

Publications

1996 Sheet Models of Protostellar Collapse, L. Hartmann, N. Calvet, & A.P. Boss, ApJ, in press

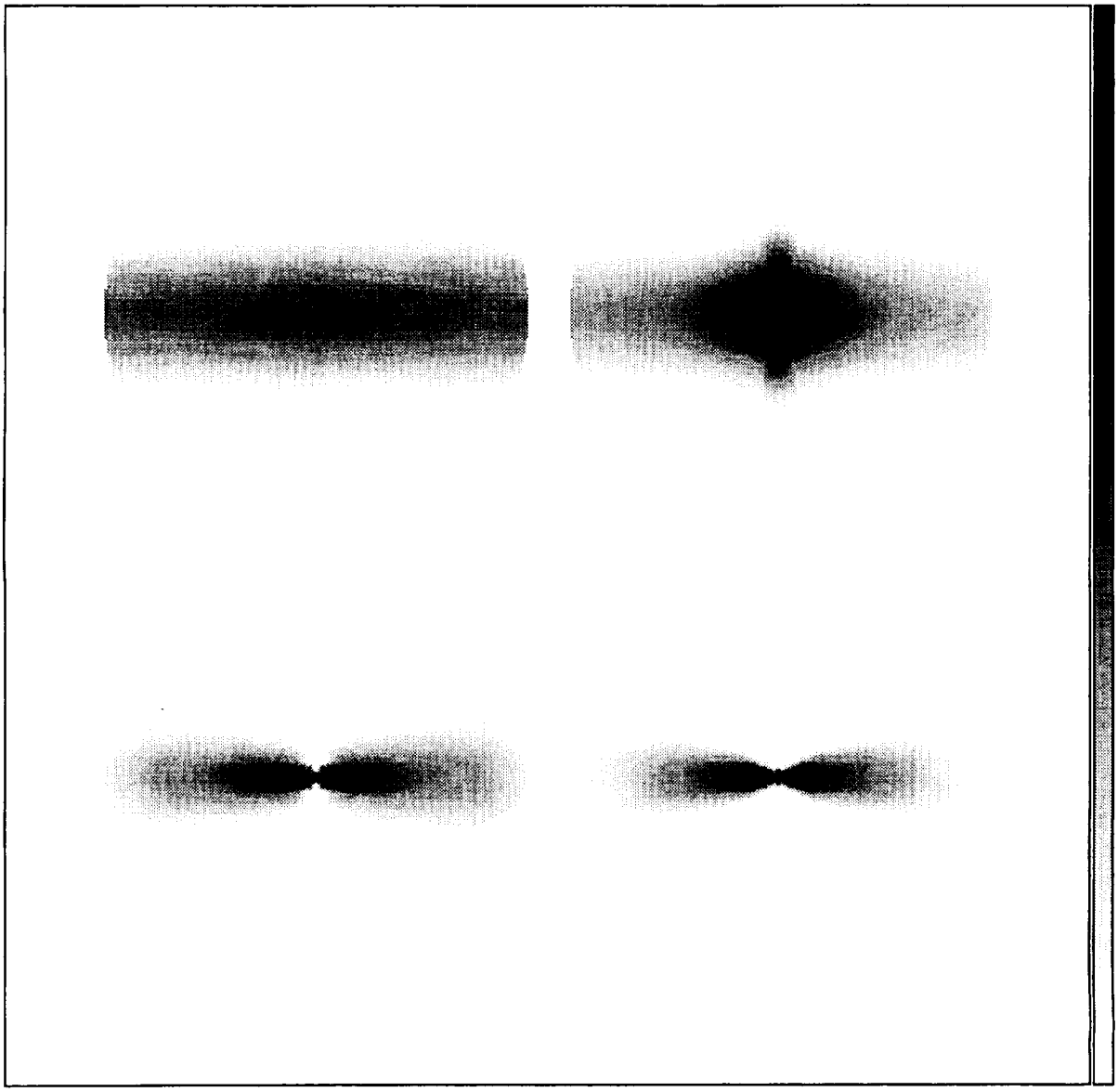

Figure 1: Gray-scale representation of the density distribution of the numerical simulation in Paper I, measured in a meridional plane. The initial density distribution is that of an isothermal self-gravitating, infinite layer; the simulation is bounded by a spherical surface that does not allow material from the outside to fall in. The radius of this surface is just large enough that the enclosed material is gravitationally unstable (see text). In the upper left, after 2.7 free-fall times ($= 1.2 \times 10^5$ yr), the layer still retains its basic hydrostatic equilibrium configuration as material begins to fall in. After 6 free fall times, a dense central concentration of modest flattening builds up (upper right). By 6.5 free-fall times (lower left), the material along the central axis has collapsed, producing an evacuated region perpendicular to the plane of the layer. The density distribution continues to flatten at 7 free-fall times (lower right), resulting in a toroidal density distribution.

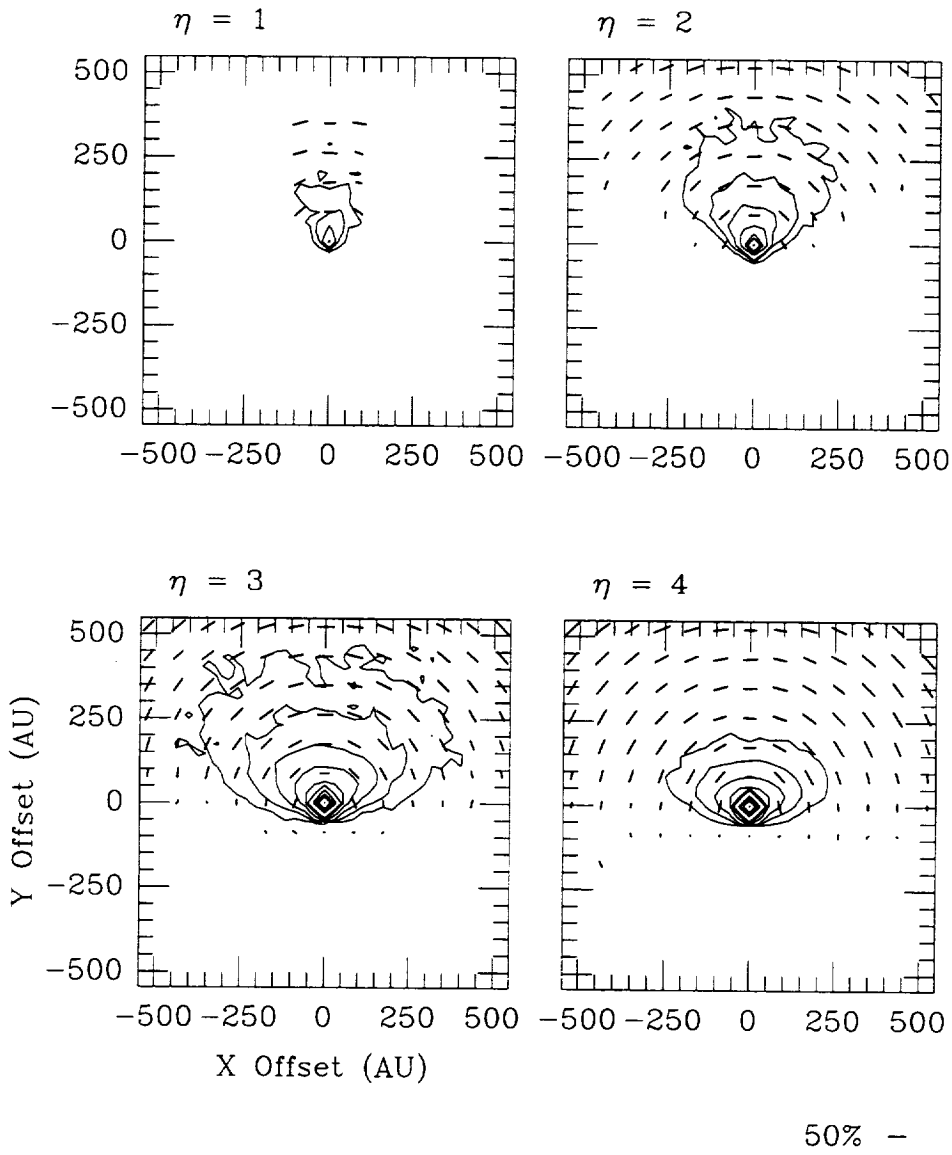

Figure 2: Images and polarization maps at 1.25μm, $i = 60°$, for the $\eta = 1, 2, 3, 4$ models with $\dot{M} = 4 \times 10^{-6} M_\odot\,\mathrm{yr}^{-1}$, $R_c = 50$ AU, and $M = 0.5 M_\odot$, assuming MRN dust parameters (see text). The opening angle of the reflection nebula increases with increasing η.

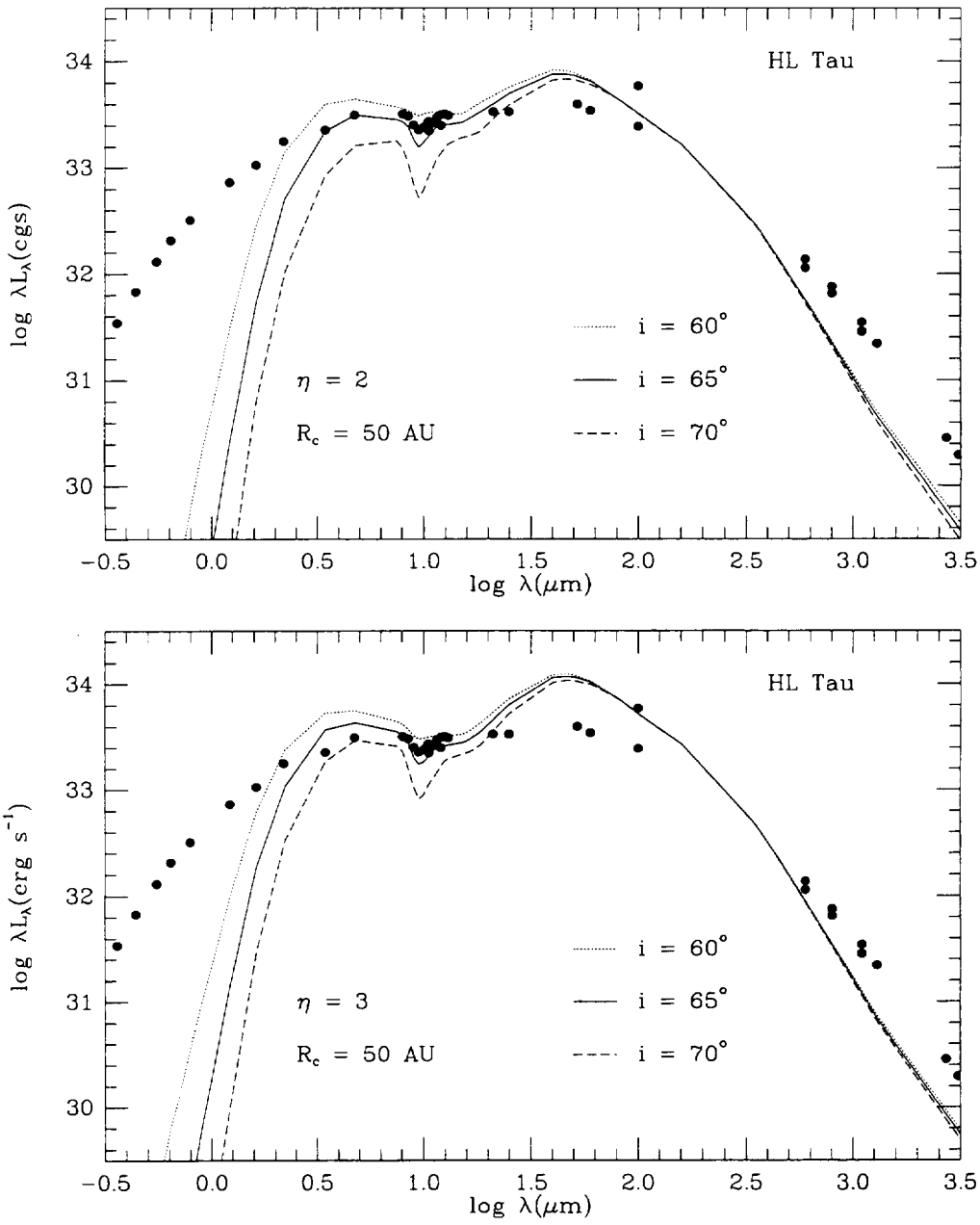

Figure 3: Spectral energy distribution of the flat-spectrum T Tauri star HL Tau (Calvet *et al.* 1994), compared with flattened collapse models with $\eta = 2, 3$ and $R_c = 50$ AU (see text)

Final Report for NAGW-2919

Mass Loss from Pre-Main Sequence Accretion Disks

Calvet, Hartmann, and Kenyon (1993) used radiative transfer models to test the disk-wind model of accretion-driven bipolar outflows (Blandford & Payne 1982; Pudritz & Norman 1983; Königl 1989; Pringle 1989; Pelletier & Pudritz 1991). To test the disk wind hypothesis by comparing with observed line profiles, wind models were constructed which account for the variable ionization and line excitation as a function of height above the disk and radial distance from the central star. A schematic velocity structure was adopted for the disk wind, calculate the wind temperature assuming radiative equilibrium, and compute line profiles assuming LTE populations for the neutral and singly-ionized metals.

The models quantitatively agree with observed profiles of a few specific lines in FU Ori with greatly differing strengths, and explain some general trends in profile shapes and asymmetries found by Petrov & Herbig (1992). The model predicts that strong lines should be asymmetric and blueshifted, while weak lines should be symmetric and double-peaked due to disk rotation, in agreement with observations. In addition, we suggest that many sharp blueshifted "shell" absorption features in FU Ori are not formed in a shell of roughly constant velocity, but rather rise in a rapidly expanding, *rotating* wind. The inference of rapid rotation supports the proposal that pre-main sequence disk winds are rotationally-driven. FU Ori may lose substantial amounts of mass over a significant area of the innermost disk ($\sim$ 10 stellar radii), which could have important implications for the structure of jets from young stellar objects. The results support the suggestion that massive winds originate from rapidly-accreting pre-main sequence accretion disks.

Envelopes around Herbig Ae/Be Stars

The Herbig Ae/Be stars are thought to be young, pre-main sequence stars of intermediate mass (Herbig 1960; Strom et al. 1972; Finkenzeller & Jankovics 1984; Finkenzeller & Mundt 1984). Recently, Hillenbrand et al. (1992) and Lada & Adams (1992) have interpreted the excess infrared emission of these young stars with circumstellar disk models similar to those that have successfully reproduced infrared excesses of the lower mass, pre-main sequence T Tauri stars (Adams, Lada, & Shu 1987; Kenyon & Hartmann 1987; Bertout, Basri, & Bouvier 1988). Hillenbrand et al. and Lada & Adams showed that circumstellar disk models which reproduce the $\sim 3\mu$m peaks in the near-infrared spectral energy distributions of Ae/Be stars must have high accretion rates, and must either be transparent in their inner regions, or have physical inner disk "holes".

To examine this problem more carefully, Hartmann, Kenyon, & Calvet (1993) calculated disk optical depths for optically thick and optically thin limits in the standard steady-state α-disk approximation (Shakura & Sunyaev 1973). For the optically thick case, we followed Calvet et al.'s (1991) methods for calculating disk model atmospheres to account for absorption of light from the central star by the disk. Our models show that disks around Ae/Be stars are likely to remain optically thick at the required accretion rates. Alternatively, the assumption of a physical hole in the disk implies either that large amounts of material pile up at $\sim$ 10 stellar radii or that $\sim$ 90% of the accretion luminosity escapes detection.

To avoid these difficulties we propose that the infrared excesses of many Ae/Be stars originate in surrounding dusty nebulae instead of circumstellar disks. We calculated spherically symmetric radiative equilibrium models of dusty envelopes. We find that such an envelope around either the primary star or a possible companion could explain the observations with appropriate parameters; however, the envelope must lie close to the star, and should be infalling, so the missing accretion luminosity problem remains. We propose that small dust grains–transiently heated to temperatures of $\sim$ 1000 K by $\sim$ 10 ev photons–produce the 3 μm excess. Sellgren (1984; see also Sellgren et al. 1985) originally advanced this explanation for the 1000 K continuum and line emission from large reflection nebulae around several hot stars. Given the difficulties of applying circumstellar disk models to Ae/Be stars, dusty nebula hypotheses deserve further consideration.

Scattered Light from Disks and Infalling Envelopes

Whitney & Hartmann (1992,1993) showed that scattered light images of young stellar objects can be reproduced by infalling envelopes rather than disks. The envelopes are assumed to have finite angular momentum and are falling in steady flow onto a disk. The model envelopes include holes, such as might be created by energetic bipolar flows. We calculate images using the Monte Carlo method to follow the light scattered from the dusty envelope and circumstellar disk, assuming that the photons originate from the central source. Adopting typical interstellar-medium dust opacities and expected mass infall rates for protostars $\dot{M} \sim 10^{-6} M_{\odot}\,yr^{-1}$, we find that detectable amounts of optical radiation can escape from envelopes falling in to a disk as small as $\sim$ 10 – 100 AU, depending upon the viewing angle and the size of the bipolar flow cavity. The models explain general features of polarization maps of many young stellar objects. In particular, parallel polarization patterns ("polarization disks") can be produced by multiple scattering effects very simply in envelopes and do not require large-scale disk structure.

The Embedded Young Stars in the Taurus-Auriga Molecular Cloud: Models for Scattered Light Images

Kenyon, Whitney, Gomez, and Hartmann (1993) collected near-IR images and calculated scattered light models for the Taurus embedded (or class I) sources. We define the embedded sources as pre-main sequence stars whose ratio of IRAS to bolometric luminosity is $L_{IRAS}/L_{bol} \gtrsim 0.8$ (Kenyon et al. 1993). The observations show a large range in J–K and H–K colors for these class I sources. The bluest objects have colors similar to the reddest T Tauri stars in the cloud; redder objects lie slightly above the reddening line for standard ISM dust and have apparent K extinctions of up to 5 mag, as shown in Figure 1. Most of these sources also show extended near-IR emission on scales of 10–20 arcsec , which corresponds to linear sizes of 1500–3000 AU. The near-IR colors and nebular morphologies for this sample and the magnitude of linear polarization in several sources suggest scattered light produces most of the near-IR emission in these objects.

We adopted the Terebey, Shu, & Cassen (1984) solution for an infalling, rotating protostellar cloud and used a two dimensional Monte Carlo radiative transfer code (Whitney & Hartmann 1992, 1993) to model the near-IR colors and images for the embedded sample. Our results suggest mass infall rates that agree with predictions for cold clouds (T $\sim$ 10–20 K) and are generally consistent with rates estimated from radiative equilibrium models of Kenyon et al. 1993a (e.g., $\dot{M} \sim 2\text{–}10 \times 10^{-6}\, M_\odot\, yr^{-1}$). For reasonable dust grain parameters, the range of colors and extinctions require flattened density distributions with polar cavities evacuated by bipolar outflows. These results support the idea that infall and outflow occur simultaneously in deeply embedded, bipolar outflow sources. The data also indicate fairly large centrifugal radii, $R_c \sim 100$ AU, and large inclinations to the rotational axis, $i \sim 60 - 90°$, for a typical source. Our centrifugal radius estimates agree with the disk radii inferred for many T Tauri stars in the Taurus-Auriga cloud. Better maps of polarization and molecular outflows in these objects can test our inclination estimates.

Spectrum of the "Invisible" Companion of Z CMa Revealed in Polarized Light

Whitney et al. (1993) obtained optical spectropolarimetry of the FU Orionis variable (FUor) Z CMa in 1991-1992 which shows larger polarization in the emission lines than in the continuum. The intensity spectrum at this time has absorption lines with some narrow weak emission. The polarized flux spectrum appears similar to an intensity spectrum of Z CMa obtained in 1987 when it was ~ 0.9 magnitudes brighter at V and showed strong emission lines. We argue that the primary component of the Z CMa binary is an emission line source, perhaps an Ae/Be star, that varies at V by 1-3 magnitudes

and was responsible for the 1987 outburst. The primary is mostly obscured from view by an asymmetrical distribution of dust which polarizes the light scattered into our line of sight. The secondary, a normal FUor, is seen more directly, and therefore contributes a large amount of unpolarized flux, about 80% of the total optical flux. Most of the polarization is intrinsic to the system and oriented perpendicular to the jet axis. We propose that independent variations in the brightness of both sources are responsible for the appearance and disappearance of a narrow emission line spectrum on the broader FUor absorption line spectrum.

Protostellar Collapse in a Self-Gravitating Sheet

We presented (Hartmann *et al.* 1995) preliminary calculations of protostellar cloud collapse starting from an isothermal, self-gravitating gaseous layer in hydrostatic equilibrium. This gravitationally unstable layer collapses into a flattened or toroidal density distribution, even in the absence of rotation or magnetic fields. We suggest that the flat infalling envelope recently observed in HL Tau by Hayashi *et al.* is the result of collapse from an initially non-spherical layer. We also speculate that the later evolution of such a flattened, collapsing envelope can produce a structure similar to the "flared disk" invoked by Kenyon and Hartmann to explain the infrared excesses of many T Tauri stars.

Magnetospheric Accretion Models for T Tauri Stars.

I. Balmer Line Profiles Without Rotation

In this paper (Hartmann, Hewett, & Calvet 1994) we showed that the strong emission lines of T Tauri stars are probably produced in infalling envelopes. Simple models of infall constrained to a dipolar magnetic field geometry explain many peculiarities of observed line profiles that are difficult, if not impossible, to reproduce with wind models. Radiative transfer effects explain why certain lines can appear quite symmetricwhile other lines simultaneously exhibit inverse P Cygni profiles, without recourse to complicated velocity fields. The success of the infall models in accounting for qualitative features of observed line profiles supports the proposal that stellar magnetospheres disrupt disk accretion in T Tauri stars, that true boundary layers are not usually present in T Tauri stars, and that the observed "blue veiling" emission arises from the base of the magnetospheric accretion column.

In Figure 1 we show the simultaneously obtained line profiles of Hβ and Hγ in BP Tau and UY Aur, compared with the non-isothermal model results for $i = 60°$. These profiles

appear to be typical, based on comparison with the observations of Basri *et al.* (1989) and Edwards *et al.* (1993b). Overall, the calculations are in reasonably good agreement with the observations. Our models are limited by the uncertainty in the magnetospheric temperature distribution, and so we concentrate on qualitative properties of the line profiles. The model profiles exhibit two properties which are particularly significant:

1. Absence of blueshifted absorption. One drawback of the infall model is that it cannot explain the blueshifted absorption seen in Hα. Conversely, an advantage of the infall model is that it predicts no blueshifted absorption in the higher Balmer lines. As Figure 12 shows, such absorption is often absent in T Tauri stars. On the other hand, models in which the Balmer emission arises in the wind generally predict very strong blueshifted absorption in the upper Balmer lines (see Figures 11-15 of Hartmann *et al.* 1990). This absorption is very difficult to avoid in simple wind models.

2. Central, slightly blueshifted emission peak. In both BP Tau and UY Aur spectra the Hβ and Hγ emission is centrally peaked and slightly blueshifted with respect to the stellar rest velocity (determined previously to better than $2\,\mathrm{km\,s^{-1}}$; Hartmann & Stauffer 1989). This is also extremely difficult to obtain with simple wind models (Figures 11-15 in Hartmann *et al.* 1990). The infall model naturally predicts central emission peaks with small blueshifts.

The observations show less or no evidence for redshifted absorption in Hγ, unlike the models. However, we showed that the amount of redshifted absorption is sensitive to the exact geometry and to the temperature of the hot ring. Our calculations show that other lines, such as the Na I resonance lines, are more likely to show the redshifted absorption, in qualitative agreement with observations.

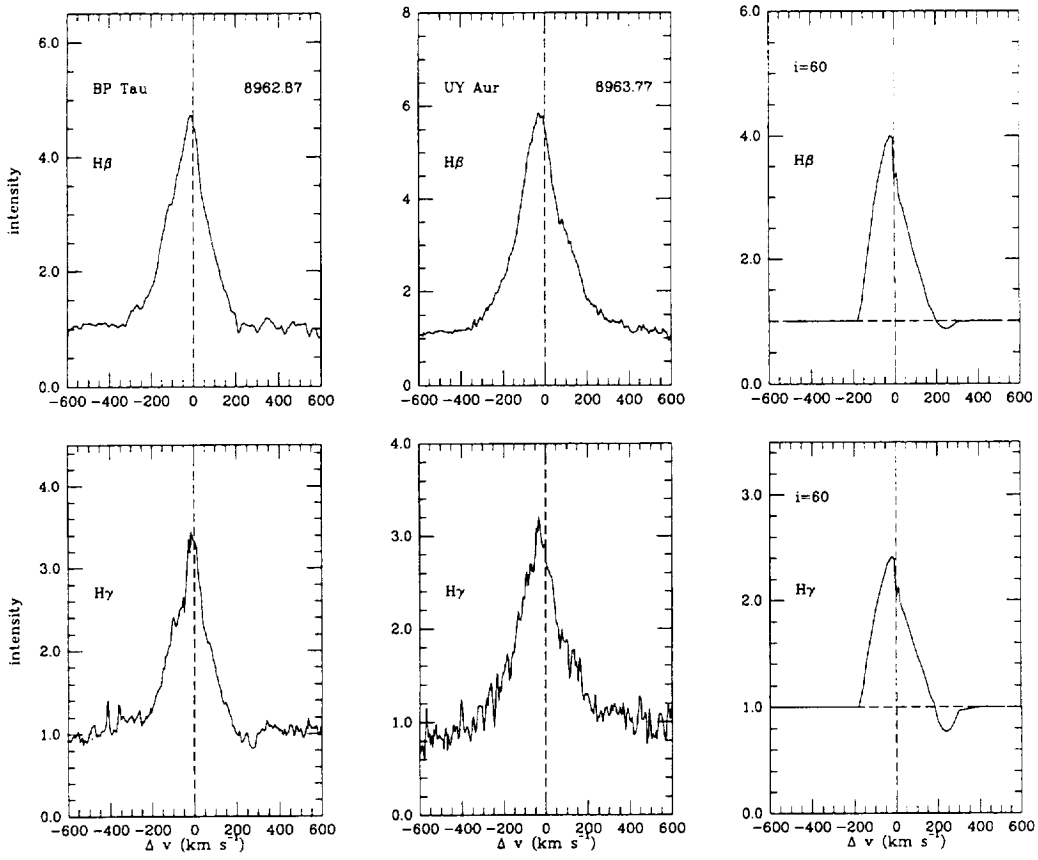

Figure 1: Comparison of observed Hβ and Hγ line profiles for BP Tau and UY Aur (see text) with model results for $i = 60°$.

Sheet Models of Protostellar Collapse

Recognizing that protostellar clouds are unlikely to be completely spherical, we explore some effects of initial cloud geometry by considering collapse from a sheet initially in hydrostatic equilibrium. A qualitatively different feature of sheet collapse compared with spherical contraction is the development of relatively evacuated cavities in the infalling dusty cloud, which arise because material falls in first along the shortest dimension to the central gravitating mass. We introduce a flattening parameter η which joins our approach with that of Terebey *et al.* (1984); $\eta = 0$ corresponds exactly to that of Terebey *et al.* , while values of $\eta \sim 2 - 3$ are indicated for typical times during the collapse of the self-gravitating isothermal sheet. This analytic models reproduces the main features of our previous numerical time-dependent simulations (see Figure 1).

We performed detailed radiative transfer calculations which suggest that these

collapse cavities can naturally explain the morphological appearance of many reflection nebulae around young stars on small distance scales without requiring initially diverging outflows (Figure 2). Sheet collapse models can simultaneously explain small-scale reflection nebula morphologies and dust envelope emission properties of many young stellar objects more easily than the standard spherical collapse models. The sheet collapse picture suggests that protostars, i.e. young stellar objects still accreting a large fraction of their mass from infalling envelopes, may be optically visible over a substantial range of system inclinations to the line of sight. These results may be especially relevant to cases where fragmentation and collapse has been triggered by an external impulse, such as a shock wave.

We showed how many properties of the flat-spectrum T Tauri star HL Tau can be intepreted in terms of flattened protostellar cloud collapse (Figure 3). Overall, our model explains the main features of the flattened infalling gas cloud found by Hayashi *et al.* (1993) from ^{13}CO interferometric mapping, the scattered light nebulae observed by Beckwith *et al.* (1989) and Beckwith & Birk (1995), the redshifted C_2 absorption found by Grasdalen *et al.* (1989), and the flat-spectral energy distribution (Calvet *et al.* 1994). The model cannot reproduce all of the fine detail seen in the Hubble Space Telescope image of HL Tau (Stapelfeldt et al. 1995), but these observations are more consistent with an infall model than with a disk.

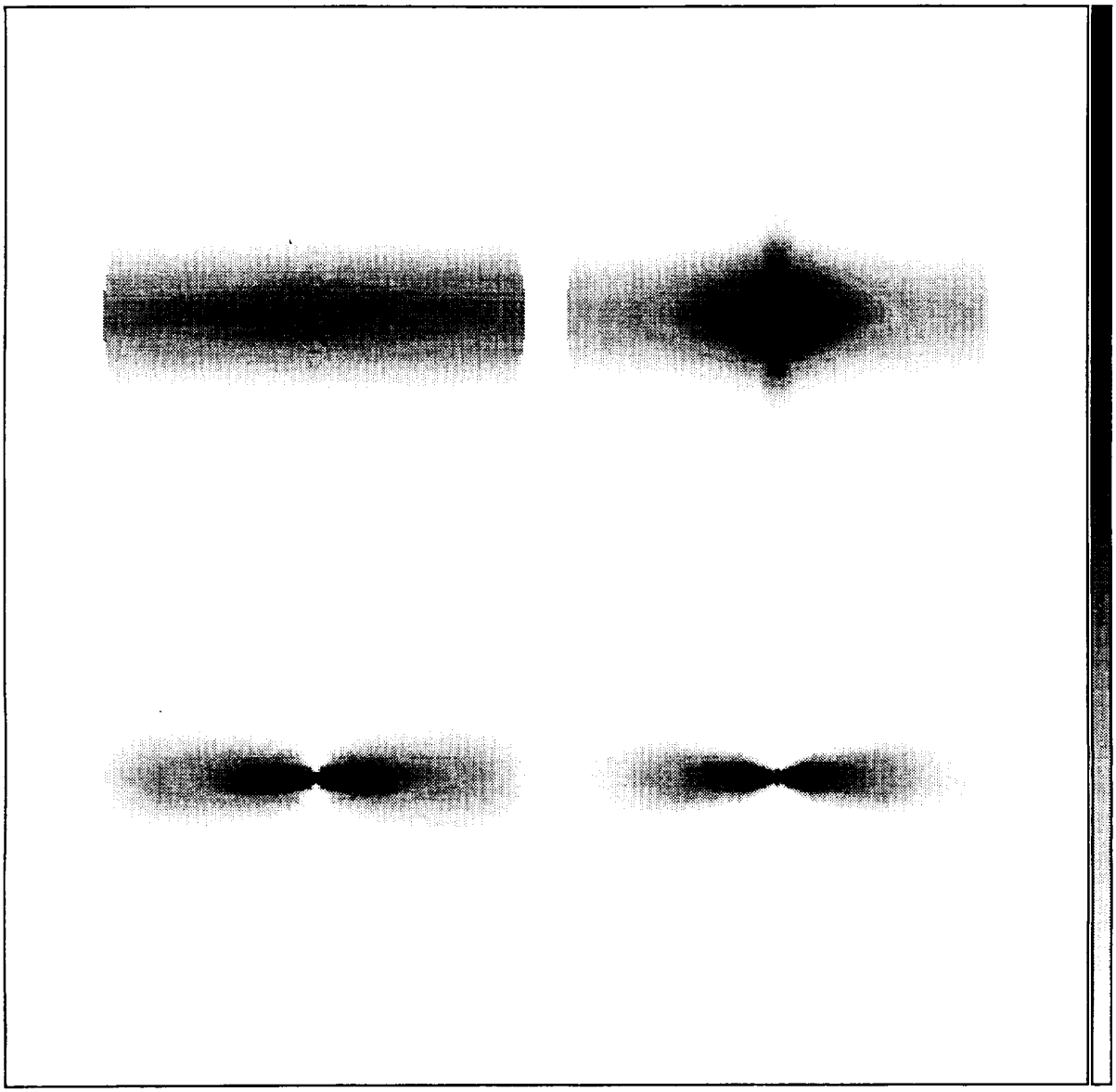

Figure 2: Gray-scale representation of the density distribution of the numerical simulation in Paper I, measured in a meridional plane. The initial density distribution is that of an isothermal self-gravitating, infinite layer; the simulation is bounded by a spherical surface that does not allow material from the outside to fall in. The radius of this surface is just large enough that the enclosed material is gravitationally unstable (see text). In the upper left, after 2.7 free-fall times ($= 1.2 \times 10^5$ yr), the layer still retains its basic hydrostatic equilibrium configuration as material begins to fall in. After 6 free fall times, a dense central concentration of modest flattening builds up (upper right). By 6.5 free-fall times (lower left), the material along the central axis has collapsed, producing an evacuated region perpendicular to the plane of the layer. The density distribution continues to flatten at 7 free-fall times (lower right), resulting in a toroidal density distribution.

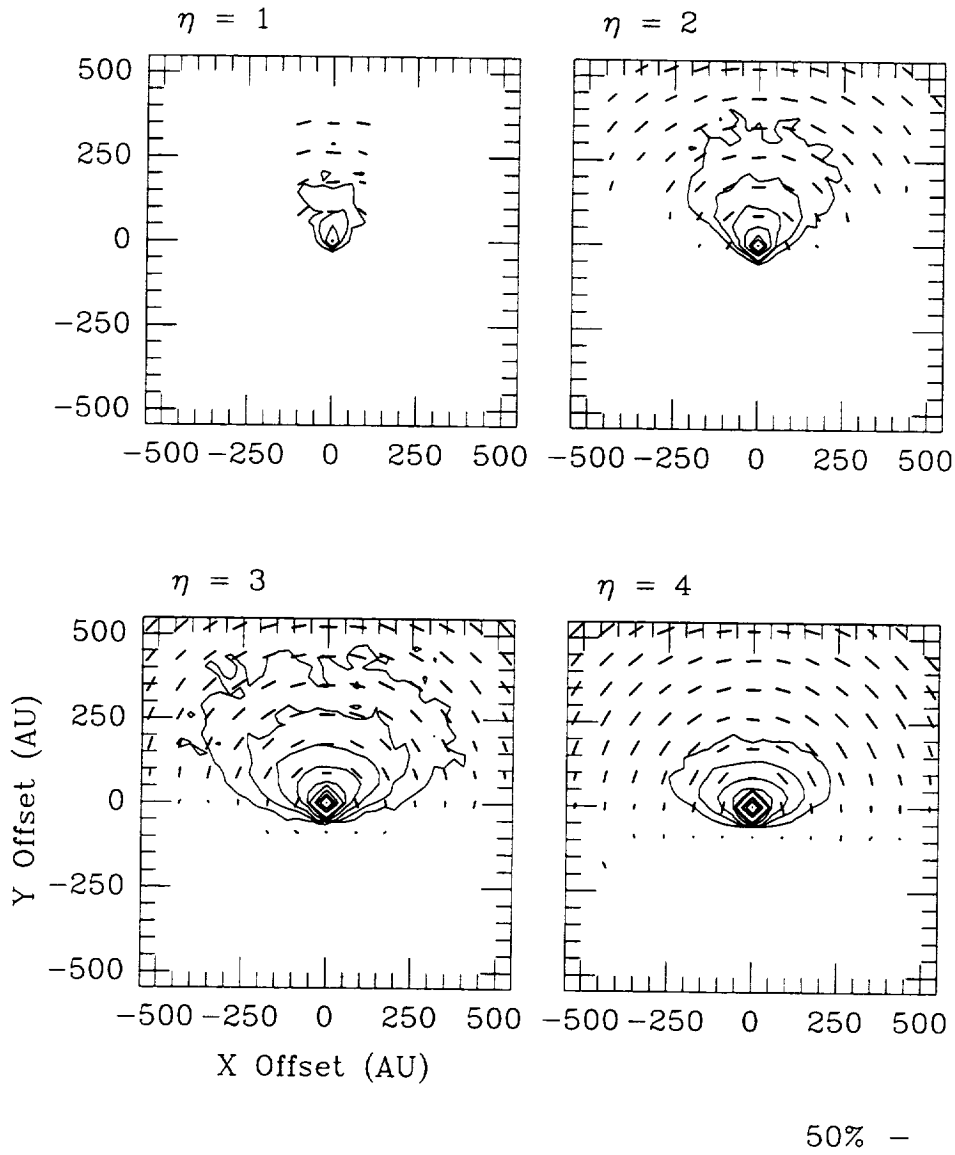

Figure 3: Images and polarization maps at 1.25μm, $i = 60°$, for the $\eta = 1, 2, 3, 4$ models with $\dot{M} = 4 \times 10^{-6} M_\odot\,yr^{-1}$, $R_c = 50$ AU, and $M = 0.5 M_\odot$, assuming MRN dust parameters (see text). The opening angle of the reflection nebula increases with increasing η.

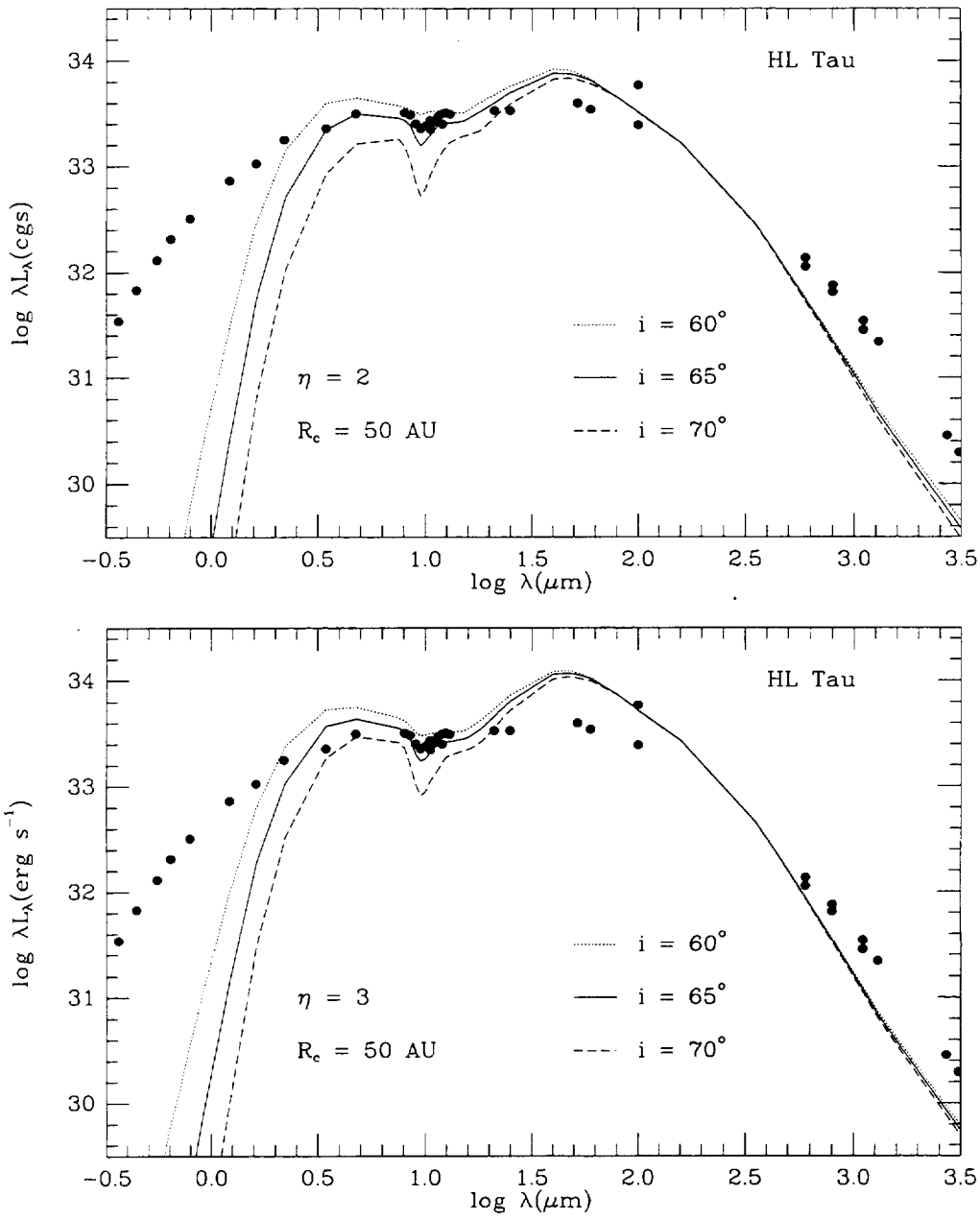

Figure 4: Spectral energy distribution of the flat-spectrum T Tauri star HL Tau (Calvet *et al.* 1994), compared with flattened collapse models with $\eta = 2, 3$ and $R_c = 50$ AU (see text)